Review article

Laser-induced hyperthermia on graphene oxide composites

Laura González-Rodríguez[a,b]*, Sara Pérez-Davila[a,b], Miriam López-Álvarez[a,b], Stefano Chiussi[a,b] , Julia Serra[a,b] and Pío González[a,b]

[a]CINTECX, Universidade de Vigo, Grupo de Novos Materiais, 36310 Vigo, Spain; [b]Galicia Sur Health Research Institute (IIS Galicia Sur), SERGAS-UVIGO, 36213 Vigo, Spain

E-mail addresses: laugonzalez@uvigo.gal; saperez@uvigo.gal; miriammsd@uvigo.gal; schiussi@uvigo.gal; jserra@uvigo.gal; pglez@uvigo.gal

Abstract

Background: Hyperthermia-based therapies have shown great potential for clinical application such as for the antitumor and antipathogenic activities. Within all strategies, the so-called photothermal therapy proposes to induce the hyperthermia by the remote laser radiation on a photothermal conversion agent, in contact with the target tissue.

Methods: This paper reviews the most relevant *in vitro* and *in vivo* studies focused on NIR laser-induced hyperthermia due to photoexcitation of graphene oxide (GO) and reduced graphene oxide (rGO). Relevant parameters such as the amount of GO/rGO, and the influence of the laser wavelength and power density are considered. Moreover, the required temperature and exposure time for each antitumor/antipathogenic case are collected and unified in a thermal dose parameter: the CEM43.

Results: The calculated CEM43 thermal doses revealed a great variability for the same type of tumor/strain. In order to detect potential tendencies, the values were classified into four ranges, varying from CEM43 < 60 min to CEM43 ≥ 1 year. Thus, a preference for moderate thermal doses of CEM43 < 1 year was detected in antitumor activity, with temperatures ≤ 50°C and exposure time ≤ 15 min. In case of the antipathogenic studies, the most used thermal dose was higher, CEM43 ≥ 1 year, with ablative hyperthermia (> 60ºC).

Conclusions: The ability of GO/rGO as effective photothermal conversion agents to promote a controlled hyperthermia is proven. The variability found for the CEM43 thermal doses on the reviewed studies reveals the potentiality to evaluate, for each application, the use of lower temperatures, by modulating time and/or repetitions in the doses.

Keywords: hyperthermia; photothermal therapy; thermal dose; near-infrared radiation; graphene oxide; reduced graphene oxide

1. Introduction

Hyperthermia refers to an increase in body temperature that can be induced by an external energy source, with the aim of achieving beneficial effects in the treatment of some pathologies and disorders (1). Among the application strategies, local hyperthermia allows the treatment of small areas with sufficient preservation of healthy tissues (2). Potential biological effects of hyperthermia were first proved by Eugene Robinson in 1974 demonstrating that heat had a selective cytotoxicity on hypoxic cells (3). Several years later this selective cytotoxicity was discovered to occur specifically in some cell types, such as cancer cells (4), due to basic physiological differences between cancerous and healthy tissue vasculature. During the same period of time, high temperatures were also proven to inhibit bacterial growth, by affecting their motility and cell wall integrity (5). In addition, Song *et al.* demonstrated in 1980 that there was a significant increase of blood flow in heated healthy tissues, indicating that hyperthermia can also induce an immune reaction or vascular stimulation, associated with the first proliferative phase of the healing process (6,7).

According to the temperature ranges applied, induced hyperthermia can be classified (8–10) as: (i) mild, when the typical physiological temperature is exceeded only by a few degrees, being 43°C the upper threshold considered for most authors; (ii) moderate, when the temperature ranges above this mild threshold but below 50°C and (iii) the ablative hyperthermia, for temperatures in the 50-55°C range, which produces the more severe effects.

Currently, most hyperthermia systems work by exposing the target tissue to energies generated by ultrasound (US) or electromagnetic (EM) radiation sources. Going into detail with electromagnetic radiation, the most commonly used systems are based on radiofrequency (RF), microwave (MW) and infrared (IR) (11). Other strategies explore the possibility of using electromagnetic radiation to irradiate photosensitive materials with the resulting release of heat. This is the case of the so-called photothermal therapy (PTT), preferably mediated by radiation in the first and second near-infrared (NIR) windows, respectively located in the 650-950 nm (NIR-I) and 1000-1350 nm wavelength ranges (NIR-IIa). At these ranges the light presents its maximum depth of penetration into the biological tissues (12), being lasers emitting at 808 nm wavelength the most widely NIR radiation sources, less expensive in relation to the ones required for NIR-II. This strategy requires short time interactions with the target tissue, and provides with spatiotemporal addressability and minimal invasiveness in comparison to chemotherapy, photocatalytic and photodynamic therapy (13–16).

Regardless of the strategy selected to induce the hyperthermia, the application of the thermal treatment involves the contribution of two basic parameters: the required temperature to be reached at the biological tissue of interest, and the application time of interaction or exposure time. These two parameters, related by a normalized method, define the so-called thermal dose, which will determine the effectiveness of the induced hyperthermia as a treatment and will allow comparison between treatments. In relation to this, and given its great importance, several mathematical models have been proposed to express that time-temperature relationship. In particular, the use of CEM43 (cumulative equivalent minutes at 43°C) stands out as a thermal dose method that finds its roots in the application of the Arrhenius model to study the kinetics of cell killing by hyperthermia. The CEM43 index, obtained using **Equation 1,** converts the various time-temperature exposures applied into an equivalent exposure time at the reference temperature of 43ºC expressed as minutes, allowing to assess the amount of tissue damage caused by heat and, consequently, its use for clinical application (17,18). With this type of tools, despite the intrinsic mathematical limitations, it is able to refine the combination of exposure time and applied temperature, therefore to manage the thermal dosimetry, for reaching an effective but safe hyperthermia effect.

$$CEM43 = \sum_{i=1}^{n} t_i \,.\, R^{(43-Ti)}$$

Equation 1. Formula for the calculation of the CEM43 parameter proposed by Dewhirst *et al*., where t_i is the *i*-th time interval, R a constant related to the applied temperature (0.25 for $T < 43$°C and 0.5 for $T > 43$°C) and T_i the average temperature during time interval t_i (19).

With respect to the materials involved in photothermal therapy (PTT), graphene derivatives have been identified as photothermal conversion agents of interest, responsible for the light-to-heat conversion. More specifically, graphene oxide (GO) and reduced graphene oxide (rGO) are the most highly investigated in the biomedical field. Their oxygen content, number of layers and lateral dimensions provide GO and rGO with improved properties with respect to graphene such as better water suspending capacity, resulting in higher biocompatibility. Moreover, they present the ability to be tailored with additional functionalities, due to the presence of reactive groups such as carboxylic acid, epoxide, and hydroxide (20). These characteristics make GO and rGO very versatile and simple to handle in aqueous media in addition to their low cost. In relation to their good ability to absorb NIR light (21–23), the photothermal conversion efficiency in the near-infrared wavelength region for graphene derivatives is estimated in about a 50%, very close to that of pure graphene and similar from those calculated for other

photothermal agents (24,25). In the specific case of GO, Savchuk and collaborators (24) estimated an efficiency of 58 ± 5% when irradiated with a wavelength of 808 nm and a laser power of 200 mW. This value is higher than the one reported by the same authors for Au nanostructures and several semiconductor materials, polymer nanostructures or nanoparticles with ferromagnetic properties for the same wavelength.

The present paper reviews the most relevant studies based on the evaluation of induced hyperthermia triggered by NIR laser photoexcitation of GO and/or rGO as a potential effective strategy for antitumor and/or antipathogenic activities. Moreover, by using the **Equation 1** above presented, the effective thermal dose CEM43, as a unifying parameter, has been determined for each of the reviewed studies, to be able to compare the obtained results for the two activities evaluated and, in this way, gain knowledge and visualize tendencies.

2. Antitumor activity

As previously mentioned, hyperthermia has been proven to generate a selective cytotoxicity, by altering the integrity of certain cells at different levels (changes in membrane permeability, protein denaturation, specific HSPs release, DNA damage…). Within the cells investigated, this selectivity was also found for cancer cells, making the hyperthermia as a potential strategy to be followed in the treatment of localized tumors.

Table 1 summarizes the reviewed papers, and main parameters provided by the authors, on the evaluation of the antitumor efficacy of PTT mediated by NIR photoexcitation of GO/rGO (26,27,36–45,28,46–55,29,56,57,30–35). The results are presented grouped by type of tumor cells evaluated, both in human and murine model lines, which are directly related to the most diagnosed cancers today: breast, cervix, prostate and lung cancer (58) and, therefore, extensively studied in all aspects. Thus, as it can be observed in **Table 1**, breast and cervical carcinoma represent almost half of the total number of papers reviewed (26,27,36–40,28–35). Prostate and lung cancer lines were also studied, although to a much lesser extent (41–43) and, finally, studies with osteosarcoma and other cancer cell lines are also included (44,45,54,56,57,46–53).

In terms of the material and laser parameters, the concentration of GO/rGO evaluated in all the mentioned studies was of up to 1mg/mL and with a preferential use of laser emitting in 808 nm. The exceptions for wavelength correspond generally to the use of others close to 808 nm, within the NIR first biological window (33,46,49,50). However, in recent years, wavelengths in the second NIR window have been explored, especially in the NIR-IIa window (1300-1400 nm)

given its superiority in penetration depth and maximum permissible exposure over NIR-I window. Thus, Xu *et al* (59) evaluated the use of laser excitation at 1275 nm demonstrating that it was practicable and exhibited, according to the authors, much more desirable outcomes in deep-tissue antitumor capabilities *in vivo* compared to that of 808 nm laser. Polyethylene glycol-stabilized copper sulfide nanoparticles were the photothermal conversion agents used at this study. Reference should also be made to the laser powers used, the influence of which was proposed by Vila *et al*. (60). Thus, these authors concluded that after irradiating osteosarcoma cell line with internalized GO, the cell culture temperature increases preferentially with laser power (from 1.5 to 3 W cm^{-2}) rather than with exposure time (from 1 to 7 minutes). Moreover, for the highest tested laser powers, necrosis was the preferential cell death, leading to an increment in cytokine release to the medium. In relation to this, it stands out that most of the reviewed studies use a wide range of power densities to determine the most adequate value for subsequent tests. In this way, most of them applied a power density lower than 5 W cm^{-2}, and only two studies, among the oldest ones, used higher power densities of up to approximately 9 W cm^{-2} (42,46).

When considering the parameters of temperature reached and exposure time (**Table 1**), the evaluation of antitumor efficacy revealed a great variability, with temperature ranging from mild hyperthermia, close to 40ºC, to ablative by applying even very high temperatures, up to 80ºC, widely exceeding therefore the 55ºC. In percentage, a 25% of the reviewed works used a temperature ≥ 55ºC. In the case of the exposure time, something similar happens, varying from minutes to one hour. At this point, due to the aforementioned variability on these both parameters, and in order to be able to compare the effectiveness of the results, the reviewed data have been unified by calculating the corresponding CEM43 thermal dose. This value has been also incorporated to **Table 1** as increasing thermal doses applied for the same type of cancer cells. On this basis, a great variability in CEM43 thermal doses is clearly observed for each type of cancer cells, with values from less than a minute to millions of years. In line with this, four ranges of CEM43 thermal dose are then proposed:

- CEM43 < 60 min, thermal dose in the range of minutes. These studies did not find significant differences in terms of cell viability (27,33,38,39,41,44,46–48,57), with the notable exception of the ones that used the Hela cell line (cervical carcinoma) (38–40).
- 1 h ≤ CEM43 < 24 h, thermal dose in the range of hours. In this case the results of these studies demonstrated a reduction of tumor cells for all the lines tested (26,28,34,35,45,49–52). However, variability was detected in the results in terms of

viability, e.g. four of these studies quantified a tumor cells viability reduction higher than 60% (26,34,50,51), while Kang *et al*. and Mun *et al*. obtained a lower reduction with values in the range of 15-25% (28,35).

- 1 day ≤ CEM43 < 365 days, thermal dose in the range of days. The results of these studies showed an effective inhibition of cancer cells viability using this higher thermal dose, with a reduction of cell viability of more than 50% in all cases (29,30,36,42,53), even reaching almost total inhibition or direct necrosis in some studies (36,42,53).
- CEM43 ≥ 1 year, thermal dose in the range of years. In these studies, the applied temperature exceeded 60ºC, which supposes a very high thermal dose with powerful results in terms of cell death (31,32,37,40,43,56).

With these four ranges in mind, it can be seen that the majority of the reviewed *in vitro* studies have selected medium thermal doses, situated in the first two ranges established: CEM43 < 60 min and 1 h ≤ CEM43 < 24 h. Despite this clear trend towards the use of CEM43 thermal doses of less than a day or few days, there is variability in the results obtained influenced, not only by the hyperthermia conditions applied, but also by the inherent differences between the cell lines. The relevance of the stage of the cell cycle and the culture conditions must be also taken into account together with the thermo-tolerance that mammalian cells develop after short periods of exposure to moderate temperatures or longer periods of exposure to sub-lethal temperatures (61–63). However, no specific differences can be elucidated depending on the origin of the cell line used.

With respect to the *in vivo* tests, a remarkable number of the reviewed studies completed their research with ectopic xenograft tumor models in small rodent, using the same cell type than *in vitro* assays. These ones have been also identified in **Table 1**. In these tests, apart from the PTT conditions applied and the strategy followed, the route of administration of the photothermal conversion agents seems to be of special relevance, being the intravenous and the intratumoral the two most common routes to administer the GO/rGO. There were exceptions such as in the research work carried out by Yan *et al.* where the subcutaneous route (51) was chosen; or at the *in vivo* evaluation presented by Sang Jung *et al.* where the compound was applied topically because a certain type of skin cancer was investigated (52). Moreover, following a different strategy, Liang Ma *et al*. manufactured a scaffold that was incorporated directly into the tumor (44). The overall analysis of the reviewed studies where an *in vivo* evaluation was carried out, shown at **Table 1**, revealed that the antitumor effectiveness achieved was mainly established based on the assessment of two parameters: variation in the tumor volume and in the animals'

total weight. Within them, two studies (26,52) indicated a total inhibition of the tumor, complete reduction in tumor volume, concluding that there was no recurrence during the following weeks. In these two cases, GO was the photothermal conversion agent used with laser conditions of 808 nm wavelength and 2 W cm^{-2} power administered, by different routes, resulting in an applied thermal dose CEM43 of 273 minutes in case of breast cancer and of 1280 minutes in melanoma. In both cases de CEM43 remained below 24 hours, in the 1 h < CEM43 < 24 h, thermal dose range. There was another study, Zhang *et al.* (34), that proposed a combination of chemotherapy and photothermal therapy in one system, using graphene oxide as photothermal agent but also as a delivery agent of a conventional antitumor drug for breast tumor. The results demonstrated that the synergistic effect significantly improved the therapeutic efficacy, and presented a lower toxicity when compared to the administration of the antitumor agent alone. The calculated CEM43 thermal dose applied at this case, where photothermal therapy was combined with chemotherapy, was lower with a value of 384 minutes, again in the range 1 h < CEM43 < 24 h range.

Table 1: Summary of the reviewed studies related to antitumor activity based on hyperthermia generated by photon excitation of GO and/or rGO in the NIR range.

In vitro cell line	Material	Laser wavelength [nm]	Power density [W cm^{-2}]	Temperature reached [°C]	Exposure time [min]	CEM43 thermal dose [min]	Results (*in vitro* assays)	*In vivo* conditions	Results (*in vivo* assays)	Ref.
4T1 breast (murine model)	GO	808	2.0	48	3	36	No significant effect is achieved without a complementary drug	-		(27)
MCF-7 breast	GO	810	1.4	35	3	1.5×10^{-5} (< 1 min)	No photothermal effect data on cells without chemotherapeutic agent	-		(33)
EMT6 breast (murine model)	GO	808	2.0	≈ 50	3	384 (6.4 h)	Cells inhibition rate of 80%	Tail vein injected 40 days treatment	PTT with GO presented the same effectiveness than the obtained with low-dose drugs, no regrow	(34)
MDA-MB-231 breast	GO	808	2.0	≈ 50	5	273 (4.5 h)	An 87% inhibition rate of cells	Tail vein injected 20 days treatment	Tumors completely inhibited, without recurrence	(26)
MDA-MB-231 breast	rGO	808	2.0	≈ 50	10	309 (5.1 h)	Viability of cancer cells significantly reduced (by about 25%)	-		(35)
MCF-7 breast	rGO	808	0.6	50	5	137 (2.3 h)	PTT effect dependent on the concentration of the material; total inhibition is	Not specified	No apparent differences *in vivo* after a single dose of radiation	(36)

							achieved with ≥ 100 mg/L			
MCF-7 breast	GO and rGO	808	2.5	≈ 80	8	≈ 2 million years	GO exhibit excellent photothermal abilities capable to eliminate effectively the 95% of cancer cells	-		(37)
Hela cervical	rGO	808	0.2	39	10	0.002 (< 1 min)	Viability in cell line used decreases to about 60%	-		(38)
Hela cervical	GO	808	0.4	≈ 41	10	0.625 (< 1 min)	Very strong inhibition of tumor cells (significantly different from 25 μg/mL)	Tail vein injected 14 days treatment	Effective tumor PTT with only one irradiation	(39)
Hela cervical	rGO	808	-	65	7	4.3×10^6 (8.2 years)	Significant elimination of cancer cells	-		(40)
Hela cervical	rGO	808	4.0	52	5	2064 (1.4 days)	Significant differences in cancer cell death (reduction of about 15%)	-		(28)
Hela cervical	GO	808	5.0	44	3	2	Significant decrease in cell viability	-		(29)
Hela cervical	rGO	808	0.6	≈ 55	10	1.1×10^4 (7.6 days)	Significant differences in cancer cell death at the highest concentration. Death of cells > 50%	-		(30)

Hela cervical	GO	808	0.72	63	10	1.1×10^7 (19.9 years)	Up to 60% reduction in cell viability	Intravenously injected	Noticeable reduction in the tumor size	(31)
Hela cervical	GO	808	2.0	79	10	6.8×10^{11} (≈ 1 million years)	More than 50% reduction in cell viability	Intratumorally injected 14 days treatment	The tumor disappeared completely	(32)
A549 lung	rGO	808	2.0	≈ 65	5	8.9×10^6 (16.9 years)	When the maximum non-cytotoxic concentration is irradiated, cancer cells viability is reduced by up to 40% and normal cells are maintained at 70%	-		(43)
PC3 prostate	GO	808	3.0	45	5	4	Trend of cells elimination but no significant differences	Intratumorally injected 15 days treatment	No improvement but tumor volume is maintained and does not grow	(41)
LNCaP prostate	GO and rGO	808	7.5	45	1	4	Decrease in cancer cells viability much more pronounced when using rGO. Almost a total death is achieved	-		(42)
HOS osteosarcoma	GO	808	2	48	5	160 (2.6 h)	The scaffold showed excellent photothermal response *in vitro*; 30% of cells in apoptosis	Scaffold implantation	The tumor volume changed and and an extensive necrosis effect appeared	(44)
MG-63 osteosarcoma	GO	808	1.5	45	8	33	Differences in viability of cells at longer exposure times	-		(45)

OE-19 esophageal	GO and rGO	808	3.0	≈ 40	10	0.05 (< 1 min)	No significant effects	-		(57)
C26 colon	rGO	785	9.62	≈ 42	10	0.77 (< 1 min)	No significant effect on cell proliferation is achieved without a complementary photothermal agent	-		(46)
KM12C colon	GO	808	0.3	≈ 42	20	1	Almost complete inhibition of cells	-		(48)
CT26 colon (murine model)	rGO	808	1.0	53	8	2340 (1.6 days)	Over 80% of cancer cells reduction	Subcutaneously injected 16 days treatment	Activation of the immune response	(51)
BEL-7402 hepatoma K-150 esophageal HCT-116 colon	GO	808	2.0	≈ 48	5	36	Inhibition of cell growth in all lines but strongest for hepatoma	Tail vein injected	Significant differences in tumor volume but without being eradicated	(54)
B16F10 melanoma (murine model)	GO and rGO	960	2	≈ 43	60	60	Cell death was confirmed by the release of lactate dehydrogenase from dead and dying tumor cells	-		(49)
A-431 epidermoid carcinoma	rGO	810	0.15	≈ 45	30	741 (12.3 h)	Cancer cells viability is reduced by up to 60%	-		(50)
B16F10 melanoma (murine model)	GO	808	2.0	≈ 50	10	1280 (21.3 h)	Drastic decrease of cells viability from 200 µg/mL and above	Topically administered	Complete ablation of tumor tissues with no recurrence	(52)
U87 MG glioblastoma	GO	808	2.0	43	3	1	Significant results in the elimination of cancer cells	-		(47)

U87 MG glioblastoma	GO and rGO	808	0.6	55	8	14884 (10.3 days)	Better photothermal capacity of rGO compared to GO. Drastic reduction of viability	-	(53)
U87 MG glioblastoma	rGO	808	2.5	≈ 55	10	9024 (6.3 days)	80% cell death is achieved	-	(56)

3. Antipathogenic activity

Infections caused by some bacterial and fungal strains are attracting great concern in the medical community because of the high mortality rates associated. Within them, Kraker *et al.* (64) highlighted the mortality and consequences caused by two particular bacterial strains: methicillin-resistant *Staphylococcus aureus* (MRSA) and third-generation cephalosporin-resistant *Escherichia coli* (G3CREC). This high mortality is due to the decreasing effectiveness of conventional treatments against these microorganisms, a process that has increased in recent decades due to various factors such as the misuse of antibiotics. This resistance, identified as one of the top 10 global public health threats (65), urges the development of alternative procedures to fight the so-called multi-drug resistant pathogens, being hyperthermia-based systems an interesting approach.

Going into detail, the two mechanisms of action that alter the integrity of microorganisms are the membrane disruption and oxidative stress. Both processes can be caused by localized hyperthermia generated by NIR irradiation of GO/rGO (66). The first effect (membrane disruption) is the result of physical damage produced by the GO/rGO nanosheets themselves. This leads to instability of the cellular structure and consequently the bacteria inactivation (67). The second effect, oxidative stress, occurs at the same time, due to the reactive oxygen species (ROS) produced by these graphene derivatives. This causes damage to cellular components, such as lipids and proteins, and with them the mitochondrial dysfunction and DNA damage, after being internalized by cells (68). Both effects are increased by the additional damages caused by hyperthermia in the same way (69).

Table 2 collects a summary of the reviewed publications, with main parameters provided by the authors, on the evaluation of the antimicrobial efficacy of PTT mediated by NIR photoexcitation of GO/rGO (70–78). Additionally, the CEM43 thermal dose has also been calculated, and incorporated for each publication. Thus, when first looking at **Table 2**, it is noted that the studies are mainly focused on the most investigated bacterial strains, above mentioned, *Staphylococcus aureus* and *Escherichia coli*. However, two of the reviewed publications (70,71) include studies with pathogenic fungi such as *Saccharomyces cerevisiae* and some species of the genus *Candida*. This latter is also considered already at the same threat level as the assigned to the above-mentioned bacteria given several evidences of drug-resistant *Candida* yeasts (79). In relation to the photothermal conversion agents, GO or rGO have been used mostly as nanosheets and nanotubes in dispersions or scaffolds. Moreover, it is also important to take into account the antimicrobial action derived solely from the presence of these

graphene derivatives, already proven at previous studies (80,81) where authors concluded that GO produces the strongest effect, followed by rGO, graphite and graphite oxide. When hyperthermia is additionally incorporated, induced by PTT using the GO/rGO as PTCAs, the reviewed publications presented at **Table 2** revealed that none of the studies used GO/rGO concentrations exceeding 100 μg/mL. When considering the laser parameters, almost all authors used a wavelength of 808 nm, as well as in the antitumor activity, which is within the *first biological window*. Two of the reviewed works (71,76) applied different wavelengths, 660 nm and 1064 nm respectively, which although not the most studied wavelengths, they both still belong to the NIR biological window. Furthermore, in relation to the power laser, it seems that the trend is moving towards the use of soft power densities ≤1.5 W cm^{-2} and, to our best knowledge, only two reviewed studies exceeded this value, using up to 3 W cm^{-2} (72,73). When considering the temperature, a clear tendency was detected on these antipathogenic studies with the application of high temperatures in the ablative range with values ≥ 55ºC in the 100% of the cases.

As in the studies for tumor cells, the thermal dose has also been calculated for the antipathogenic reviewed works presented at **Table 2**, using the CEM43 parameter. It can be observed (**Table 2**) that the thermal doses applied are very high, 77.8% in the range CEM43 ≥ 1 year (70–73,76–78) and 22.2% in the 1 day ≤ CEM43 < 365 days' range (74,75). These high thermal doses are generated by the use of high temperatures, included in the ablation range (≥55ºC), combined with exposure times of great variability from 3 to even 60 minutes. The use of such high temperatures can be justified by the recently demonstrated effect on the morphology of the biofilm formed by *Staphylococcus* bacteria when exposed to local heating above 60°C and for long periods of time (82). According to the biological response to these thermal doses, a very strong decrease in microbial viability was achieved in all *in vitro* tests. However, only three of the reviewed works carried out animal experiments and offered promising results with an enhanced reduction of bacterial infection (70,71,76). Moreover, these three *in vivo* studies observed a simultaneous acceleration of the wound healing, with faster healing of skin wounds compared to the control probes in both, mouse and rat populations. Additionally, Li and collaborators (76) claimed the absence of toxicity of their strategy, based on a composite with Zn and GO and dual light irradiation for 10 minutes, to organs and proposed some regulatory mechanisms that may occur. Finally, clear positive antipathogenic results were observed from the first days of treatment by Wu *et al*. (70), who also claimed that the injuries of rats treated with the GO composite did not show erythema symptoms.

Table 2: Summary of the reviewed studies related to antipathogenic activity based on hyperthermia generated by photon excitation of GO and/or rGO in the NIR range.

Type of microorganism	Material	Laser Wavelength [nm]	Power Density [W cm^{-2}]	Temperature reached [°C]	Exposure Time [min]	CEM43 thermal dose [min]	*In vivo*	Results	Ref.
S. aureus	rGO	808	0.4	60	10	1.3 x 10^6 (2.5 years)	-	Almost 100% killing efficiency and maintained even after storage for 30 days	(77)
E. coli	GO	808	2.78	65	5	2.1 x 10^7 (39.9 years)	-	Total antibacterial capability >98%	(73)
S. aureus and *E. coli*	GO	808	1.5	55	5	5281 (3.6 days)	-	Almost complete elimination of bacteria	(74)
S. aureus and *E. coli*	GO	808	0.6	55	60	2.4 x 10^5 (170 days)	-	Antibacterial effect of 99.91%	(75)
S. aureus and *E. coli*	GO	660	0.9	65	10	2.7 x 10^7 (52.3 years)	14 days treatment	Significant differences in antibacterial potential of up to 54% for *S. aureus* and 66% for *E. coli*	(76)
S. aureus and *E. coli*	rGO	808	3.0	70	6	8.0 x 10^8 (thousands of years)	-	Bacterial viability reduced to 0%	(72)

E. coli and *S. typhimurium*	GO	808	-	66	15	6.4×10^7 (122.2 years)	-	Effective killing (>95%)	(78)
S. aureus and *P. aeruginosa* *S. cerevisiae* and *C. albicans*	GO	808	1.0	61	6	1.6×10^6 (2.9 years)	21 days treatment	Significant differences *in vitro* and *in vivo* results. Topical GO incorporation and daily irradiation had effective potential	(70)
S. aureus and *P. aeruginosa* *S. cerevisiae* and *C. utilis*	GO	1064	-	64	3	6.3×10^6 (11.9 years)	6 days treatment	Not only the *in vivo* infection is stopped but also the wound healing is improved	(71)

4. Concluding remarks and future perspectives

As clearly documented in the present review, both graphene derivatives, GO and rGO, show a remarkable ability as effective photothermal agents when irradiated with NIR lasers and can be used in a controlled hyperthermia process. Moreover, based on the data of temperature and exposure time collected from the reviewed studies, the unified thermal dose parameter CEM43 allowed differentiating four ranges of interaction heat-cell in three thresholds: 1 hour, 1 day and 1 year. **Figure 1** presents the CEM43 thermal dose ranges established based on these three thresholds: CEM43 < 60 min, 1 h ≤ CEM43 < 24 h, 1 day ≤ CEM43 < 365 days and CEM43 ≥ 1 year, together with the position of the thermal dose calculated for each of the reviewed studies. From it, despite the variability, the preference for a certain thermal dose depending on the cell type to be irradiated (tumor cell/pathogen) is revealed. Being the moderate thermal doses of CEM43 < 1 year the most used for antitumor activity (dotted oval: black spots), with most temperatures ≤ 50°C and exposure time ≤ 15 min. While, in case of the antipathogenic studies (dotted oval: white squares), the most used thermal dose was higher, CEM43 ≥ 1 year, with ablative hyperthermia (> 60ºC). Finally, observing those two tendencies and each range values, the interest of extended research on the application of lower thermal doses: CEM43 < 1 hour for antitumor activity and CEM43 < 1 year for antipathogenic activity is clear. The efficient application of lower temperatures by modulating the thermal dose with the time of exposure and/or repetitions in the doses will also contribute to reduce the damage on surrounding tissues.

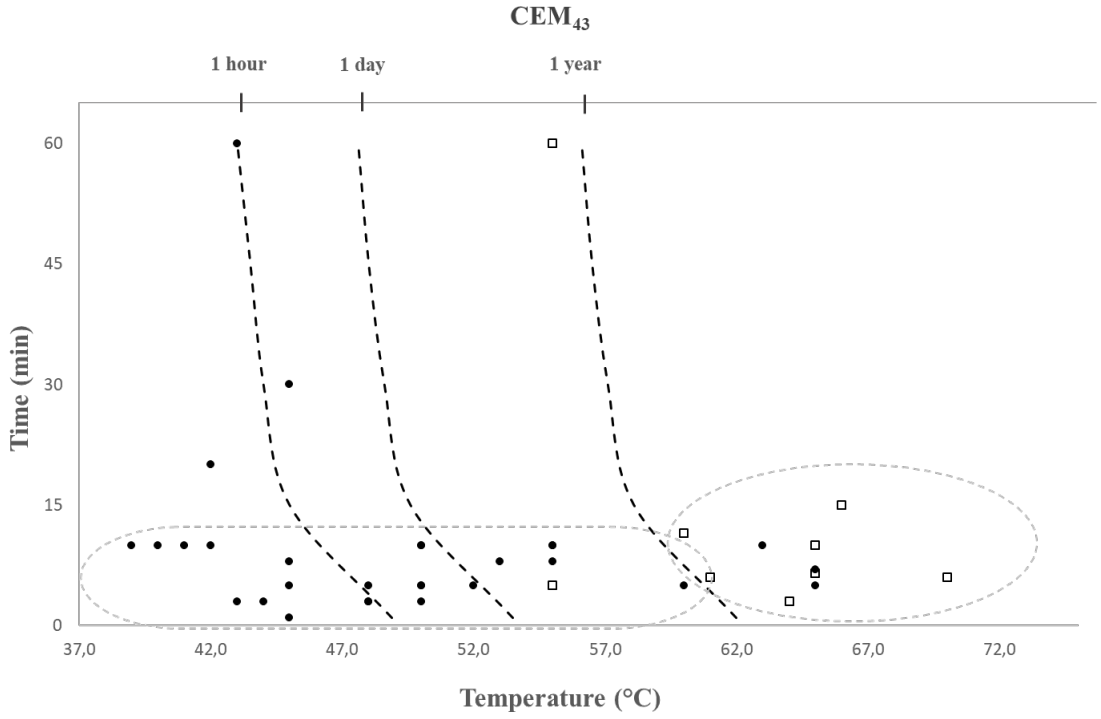

Figure 1. Graph showing the different ranges of CEM43 thermal dose and the position of those used by all reviewed studies, calculated according to equation 1. The dotted ovals encompass the thermal doses used by most of the reviewed studies, with antitumor application represented by black spots and antipathogenic studies represented by white squares.

Ethics approval and consent to participate: Not applicable

Consent to publication: Not applicable

Availability of data and materials: Not applicable

Funding for open access charge: Universidade de Vigo/CISUG.

Authors´ contributions: L.G-R., J.S. and P.G. contributed to the conception and design of the article; L.G-R. also searched for, interpreted the relevant literature, collected the data and wrote the paper. S.P-D., M.L-A. and S.C. critically reviewed the paper, as well as contributed to corrections, new ideas and approaches.

Acknowledgements: This research was financially supported by the projects BIOHEAT (PID 2020-115415RB-100) from Ministerio de Ciencia e Innovación del Gobierno de España, and the GRC support program (ED431C 2021/49) from Xunta de Galicia.

Conflict of Interest: The authors have no conflicts of interest to declare.

References

1. Mallory M, Gogineni E, Jones GC, Greer L, Simone CB. Therapeutic hyperthermia: The old, the new, and the upcoming. Crit Rev Oncol Hematol. 2016;97:56–64.
2. Chicheł A, Skowronek J, Kubaszewska M, Kanikowski M. Hyperthermia - Description of a method and a review of clinical applications. Reports Pract Oncol Radiother [Internet]. 2007;12(5):267–75. Available from: http://dx.doi.org/10.1016/S1507-1367(10)60065-X
3. Robinson J, Wizenberg M, M. & McCready W. Combined hyperthermia and radiation suggest an alternative to heavy particle therapy for reduced oxygen enhancement ratios. Nature. 1974;251:521–2.
4. Song CW, Lokshina A, Rhee JG, Patten M, Levitt SH. Implication of Blood Flow in

Hyperthermic Treatment of Tumors. IEEE Trans Biomed Eng. 1984;BME-31(1):9–16.

5. Tsuchido T, Katsui N, Takeuchi A, Takano M, Shibasaki I. Destruction of the outer membrane permeability barrier of Escherichia coli by heat treatment. Appl Environ Microbiol. 1985;50(2):298–303.

6. Song CW, Kang MS, Rhee JG, Levitt SH. The effect of hyperthermia on vascular function, pH, and cell survival. Radiology. 1980;137(3):795–803.

7. Borráez Segura B.A., Díez Rivera M.C. RICE. Fundamentos de Cirugía General. Editorial Universidad Tecnológica de Pereira; 2020.

8. Wang S, Weng J, Fu X, Lin J, Fan W, Lu N, et al. Black phosphorus nanosheets for mild hyperthermia-enhanced chemotherapy and chemo-photothermal combination therapy. Nanotheranostics. 2017;1(2):208–16.

9. Brace C. Thermal tumor ablation in clinical use. IEEE Pulse. 2011;2(5):28–38.

10. Zhang B, Wang Y, Liu J, Zhai G. Recent Developments of Phototherapy Based on Graphene Family Nanomaterials. Curr Med Chem. 2016;24(3):268–91.

11. Habash RWY. Therapeutic hyperthermia [Internet]. 1st ed. Vol. 157, Handbook of Clinical Neurology. Elsevier B.V.; 2018. 853–868 p. Available from: http://dx.doi.org/10.1016/B978-0-444-64074-1.00053-7

12. Oh J, Yoon H, Park JH. Nanoparticle platforms for combined photothermal and photodynamic therapy. Biomed Eng Lett. 2013;3(2):67–73.

13. Gollavelli G, Ghule A V., Ling YC. Multimodal Imaging and Phototherapy of Cancer and Bacterial Infection by Graphene and Related Nanocomposites. Molecules. 2022;27(17).

14. Zhang X, Wang S, Cheng G, Yu P, Chang J. Light-Responsive Nanomaterials for Cancer Therapy. Engineering [Internet]. 2022;13:18–30. Available from: https://doi.org/10.1016/j.eng.2021.07.023

15. Du T, Cao J, Xiao Z, Liu J, Wei L, Li C, et al. Van-mediated self-aggregating photothermal agents combined with multifunctional magnetic nickel oxide nanoparticles for precise elimination of bacterial infections. J Nanobiotechnology [Internet]. 2022;20(1):1–21. Available from: https://doi.org/10.1186/s12951-022-01535-1

16. Song C, Li F, Guo X, Chen W, Dong C, Zhang J, et al. Gold nanostars for cancer cell-targeted SERS-imaging and NIR light-triggered plasmonic photothermal therapy (PPTT) in the first and second biological windows. J Mater Chem B. 2019;7(12):2001–8.

17. Assi HTI, Arsenault MG, Whelan WM, Kumaradas JC. A new thermal dose model based on Vogel-Tammann-Fulcher behaviour in thermal damage processes. Int J Hyperth [Internet]. 2022;39(1):697–705. Available from: https://doi.org/10.1080/02656736.2022.2065367

18. Van Rhoon GC. Is CEM43 still a relevant thermal dose parameter for hyperthermia treatment monitoring? Int J Hyperth. 2016;32(1):50–62.

19. Dewhirst MW, Viglianti BL, Lora-Michiels M, Hanson M, Hoopes PJ. Basic principles of thermal dosimetry and thermal thresholds for tissue damage from hyperthermia. Int J Hyperth. 2003;19(3):267–94.

20. Zhang B, Wang Y, Zhai G. Biomedical applications of the graphene-based materials. Mater Sci Eng C [Internet]. 2016;61:953–64. Available from: http://dx.doi.org/10.1016/j.msec.2015.12.073

21. Muazim K, Hussain Z. Graphene oxide — A platform towards theranostics. Mater Sci Eng C [Internet]. 2017;76:1274–88. Available from: http://dx.doi.org/10.1016/j.msec.2017.02.121

22. Yang K, Zhang S, Zhang G, Sun X, Lee ST, Liu Z. Graphene in mice: Ultrahigh in vivo tumor uptake and efficient photothermal therapy. Nano Lett. 2010;10(9):3318–23.

23. Renteria JD, Ramirez S, Malekpour H, Alonso B, Centeno A, Zurutuza A, et al. Strongly Anisotropic Thermal Conductivity of Free-Standing Reduced Graphene Oxide Films Annealed at High Temperature. Adv Funct Mater. 2015;25(29):4664–72.

24. Savchuk OA, Carvajal JJ, Massons J, Aguiló M, Díaz F. Determination of photothermal conversion efficiency of graphene and graphene oxide through an integrating sphere method. Carbon N Y. 2016;103:134–41.

25. Huang Q, Li MY, Wang LL, Yuan H, Wang M, Wu Y, et al. Synthesis of novel cyclodextrin-modified reduced graphene oxide composites by a simple hydrothermal method. RSC Adv. 2018;8(66):37623–30.

26. Jun SW, Manivasagan P, Kwon J, Nguyen VT, Mondal S, Ly CD, et al. Folic acid–

conjugated chitosan-functionalized graphene oxide for highly efficient photoacoustic imaging-guided tumor-targeted photothermal therapy. Int J Biol Macromol [Internet]. 2020;155:961–71. Available from: https://doi.org/10.1016/j.ijbiomac.2019.11.055

27. Wang Y, Zhang H, Xie J, Liu Y, Wang S, Zhao Q. Three dimensional mesoporous carbon nanospheres as carriers for chemo-photothermal therapy compared with two dimensional graphene oxide nanosheets. Colloids Surfaces A Physicochem Eng Asp [Internet]. 2020;590(January):124498. Available from: https://doi.org/10.1016/j.colsurfa.2020.124498

28. Kang S, Hong YL, Ku BC, Lee S, Ryu S, Min DH, et al. Synthesis of biologically-active reduced graphene oxide by using fucoidan as a multifunctional agent for combination cancer therapy. Nanotechnology. 2018;29(47).

29. Lim JH, Kim DE, Kim EJ, Ahrberg CD, Chung BG. Functional Graphene Oxide-Based Nanosheets for Photothermal Therapy. Macromol Res. 2018;26(6):557–65.

30. Maddinedi SB, Sonamuthu J, SuzuK Yildiz S, Han G, Cai Y, Gao J, et al. Silk sericin induced fabrication of reduced graphene oxide and its in-vitro cytotoxicity, photothermal evaluation. J Photochem Photobiol B Biol [Internet]. 2018;186(July):189–96. Available from: https://doi.org/10.1016/j.jphotobiol.2018.07.020

31. Gulzar A, Xu J, Yang D, Xu L, He F, Gai S, et al. Nano-graphene oxide-UCNP-Ce6 covalently constructed nanocomposites for NIR-mediated bioimaging and PTT/PDT combinatorial therapy. Dalt Trans. 2018;47(11):3931–9.

32. Zhang X, Luo L, Li L, He Y, Cao W, Liu H, et al. Trimodal synergistic antitumor drug delivery system based on graphene oxide. Nanomedicine Nanotechnology, Biol Med [Internet]. 2019;15(1):142–52. Available from: http://dx.doi.org/10.1016/j.nano.2018.09.008

33. Mauro N, Scialabba C, Agnello S, Cavallaro G, Giammona G. Folic acid-functionalized graphene oxide nanosheets via plasma etching as a platform to combine NIR anticancer phototherapy and targeted drug delivery. Mater Sci Eng C [Internet]. 2020;107(July 2019):110201. Available from: https://doi.org/10.1016/j.msec.2019.110201

34. Zhang W, Guo Z, Huang D, Liu Z, Guo X, Zhong H. Synergistic effect of chemo-

photothermal therapy using PEGylated graphene oxide. Biomaterials [Internet]. 2011;32(33):8555–61. Available from: http://dx.doi.org/10.1016/j.biomaterials.2011.07.071

35. Mun SG, Choi HW, Lee JM, Lim JH, Ha JH, Kang MJ, et al. rGO nanomaterial-mediated cancer targeting and photothermal therapy in a microfluidic co-culture platform. Nano Converg [Internet]. 2020;7(1). Available from: https://doi.org/10.1186/s40580-020-0220-3

36. Zhang Y jin, Li B an, Li Z yuan, xia N, Yu H ying, Zhang Y zhi. Synthesis and characterization of Tamoxifen citrate modified reduced graphene oxide nano sheets for breast cancer therapy. J Photochem Photobiol B Biol [Internet]. 2018;180(December 2017):68–71. Available from: https://doi.org/10.1016/j.jphotobiol.2017.12.017

37. Li C, Chen X, Zhang Z, Jiang G. Synthesis of Neogambogic Acid Mediated Reduced Graphene Oxide Nanosheets as Photothermal Radiotherapy Agents and Effect on Breast Cancer Cells. J Clust Sci [Internet]. 2020;31(5):1097–102. Available from: https://doi.org/10.1007/s10876-019-01717-2

38. Chang G, Wang Y, Gong B, Xiao Y, Chen Y, Wang S, et al. Reduced graphene oxide/amaranth extract/AuNPs composite hydrogel on tumor cells as integrated platform for localized and multiple synergistic therapy. ACS Appl Mater Interfaces. 2015;7(21):11246–56.

39. Chang X, Zhang M, Wang C, Zhang J, Wu H, Yang S. Graphene oxide / BaHoF5 / PEG nanocomposite for dual-modal imaging and heat shock protein inhibitor-sensitized tumor photothermal therapy. Carbon N Y [Internet]. 2020;158:372–85. Available from: https://doi.org/10.1016/j.carbon.2019.10.105

40. Ma Y, Yan F, Liu L, Wei WJ, Zhao Z, Sun J. The enhanced photo-thermal therapy of Surface improved photoactive cadmium sulfide (CdS) quantum dots entrenched graphene oxide nanoflakes in tumor treatment. J Photochem Photobiol B Biol [Internet]. 2019;192(26):34–9. Available from: https://doi.org/10.1016/j.jphotobiol.2018.12.014

41. Thapa RK, Soe ZC, Ou W, Poudel K, Jeong JH, Jin SG, et al. Palladium nanoparticle-decorated 2-D graphene oxide for effective photodynamic and photothermal therapy of prostate solid tumors. Colloids Surfaces B Biointerfaces [Internet]. 2018;169(May):429–37. Available from:

https://doi.org/10.1016/j.colsurfb.2018.05.051

42. Akhavan O, Ghaderi E, Aghayee S, Fereydooni Y, Talebi A. The use of a glucose-reduced graphene oxide suspension for photothermal cancer therapy. J Mater Chem. 2012;22(27):13773–81.

43. Wang C, Wang X, Chen Y, Fang Z. In-vitro photothermal therapy using plant extract polyphenols functionalized graphene sheets for treatment of lung cancer. J Photochem Photobiol B Biol [Internet]. 2020;204(415):111587. Available from: https://doi.org/10.1016/j.jphotobiol.2019.111587

44. Ma L, Feng X, Liang H, Wang K, Song Y, Tan L, et al. A novel photothermally controlled multifunctional scaffold for clinical treatment of osteosarcoma and tissue regeneration. Mater Today [Internet]. 2020;36(xx):48–62. Available from: https://doi.org/10.1016/j.mattod.2019.12.005

45. Sang R, Chen M, Yang Y, Li Y, Shi J, Deng Y, et al. HAp@GO drug delivery vehicle with dual-stimuli-triggered drug release property and efficient synergistic therapy function against cancer. J Biomed Mater Res - Part A. 2019;107(10):2296–309.

46. Zaharie-Butucel D, Potara M, Suarasan S, Licarete E, Astilean S. Efficient combined near-infrared-triggered therapy: Phototherapy over chemotherapy in chitosan-reduced graphene oxide-IR820 dye-doxorubicin nanoplatforms. J Colloid Interface Sci [Internet]. 2019;552:218–29. Available from: https://doi.org/10.1016/j.jcis.2019.05.050

47. Kargar S, Khoei S, Khoee S, Shirvalilou S, Mahdavi SR. Evaluation of the combined effect of NIR laser and ionizing radiation on cellular damages induced by IUdR-loaded PLGA-coated Nano-graphene oxide. Photodiagnosis Photodyn Ther [Internet]. 2018;21(September 2017):91–7. Available from: https://doi.org/10.1016/j.pdpdt.2017.11.007

48. He S, Li J, Chen M, Deng L, Yang Y, Zeng Z, et al. Graphene oxide-template gold nanosheets as highly efficient near-infrared hyperthermia agents for cancer therapy. Int J Nanomedicine. 2020;15:8451–63.

49. Podolska MJ, Barras A, Alexiou C, Frey B, Gaipl U, Boukherroub R, et al. Graphene Oxide Nanosheets for Localized Hyperthermia—Physicochemical Characterization, Biocompatibility, and Induction of Tumor Cell Death. Cells. 2020;9:776–94.

50. Costa-Almeida R, Bogas D, Fernandes JR, Timochenco L, Silva FALS, Meneses J, et

al. Near-infrared radiation-based mild photohyperthermia therapy of non-melanoma skin cancer with PEGylated reduced nanographene oxide. Polymers (Basel). 2020;12(8):1–19.

51. Yan M, Liu Y, Zhu X, Wang X, Liu L, Sun H, et al. Nanoscale Reduced Graphene Oxide-Mediated Photothermal Therapy Together with IDO Inhibition and PD-L1 Blockade Synergistically Promote Antitumor Immunity. ACS Appl Mater Interfaces. 2019;11(2):1876–85.

52. Jung HS, Kong WH, Sung DK, Lee MY, Beack SE, Keum DH, et al. Nanographene oxide-hyaluronic acid conjugate for photothermal ablation therapy of skin cancer. ACS Nano. 2014;8(1):260–8.

53. Robinson JT, Tabakman SM, Liang Y, Wang H, Sanchez Casalongue H, Vinh D, et al. Ultrasmall reduced graphene oxide with high near-infrared absorbance for photothermal therapy. J Am Chem Soc. 2011;133(17):6825–31.

54. Wen C, Cheng R, Gong T, Huang Y, Li D, Zhao X, et al. β-Cyclodextrin-cholic acid-hyaluronic acid polymer coated Fe3O4-graphene oxide nanohybrids as local chemo-photothermal synergistic agents for enhanced liver tumor therapy. Colloids Surfaces B Biointerfaces [Internet]. 2021;199(November 2020):111510. Available from: https://doi.org/10.1016/j.colsurfb.2020.111510

55. Wu J, Li Z, Li Y, Pettitt A, Zhou F. Photothermal effects of reduced graphene oxide on pancreatic cancer. Technol Cancer Res Treat. 2018;17:1–7.

56. Chen X, Li C, Wang X, Zhao X. Infrared heating of reduced graphene oxide nanosheets as photothermal radiation therapeutic agents for tumor regressions. Mater Res Express. 2019;6(8).

57. Gai L-X, Wang W-Q, Wu X, Su X-J, Yang F-C. NIR absorbing reduced graphene oxide for photothermal radiotherapy for treatment of esophageal cancer. J Photochem Photobiol B Biol [Internet]. 2019 May;194(6):188–93. Available from: https://doi.org/10.1016/j.jphotobiol.2019.03.014

58. GLOBOCAN. International Agency for Research on Cancer. Cancer Today. [Internet]. Estimated age-standardized incidence rates (World) in 2020, worldwide, both sexes, all ages. 2020 [cited 2021 Jan 8]. Available from: https://www.iarc.who.int/

59. Wu X, Suo Y, Shi H, Liu R, Wu F, Wang T, et al. Deep-Tissue Photothermal Therapy

Using Laser Illumination at NIR-IIa Window. Nano-Micro Lett [Internet]. 2020;12(1):1–13. Available from: https://doi.org/10.1007/s40820-020-0378-6

60. Vila M, Matesanz MC, Gonçalves G, Feito MJ, Linares J, Marques PAAP, et al. Triggering cell death by nanographene oxide mediated hyperthermia. Nanotechnology. 2014;25(3).

61. Bhuyan BK, Day KJ, Edgerton CE, Ogunbase O. Sensitivity of Different Cell Lines and of Different Phases in the Cell Cycle to Hyperthermia. Cancer Res. 1977;37(10):3780–4.

62. Raaphorst GP, Romano SL, Mitchell JB, Bedford JS, Dewey WC. Intrinsic differences in heat and/or x-ray sensitivity of seven mammalian cell lines cultured and treated under identical conditions. Cancer Res. 1979;39(February):396–401.

63. Lepock JR. Cellular effects of hyperthermia: Relevance to the minimum dose for thermal damage. Int J Hyperth. 2003;19(3):252–66.

64. de Kraker MEA, Davey PG, Grundmann H. Mortality and hospital stay associated with resistant Staphylococcus aureus and Escherichia coli bacteremia: Estimating the burden of antibiotic resistance in Europe. PLoS Med. 2011;8(10).

65. WHO WHO. Antimicrobial resistance [Internet]. 2021 [cited 2022 Sep 23]. Available from: https://www.who.int/news-room/fact-sheets/detail/antimicrobial-resistance

66. Shi L, Chen J, Teng L, Wang L, Zhu G, Liu S, et al. The Antibacterial Applications of Graphene and Its Derivatives. Small. 2016;12(31):4165–84.

67. Li X, Li F, Gao Z, Fang L. Toxicology of graphene oxide nanosheets against Paecilomyces catenlannulatus. Bull Environ Contam Toxicol [Internet]. 2015;95(1):25–30. Available from: http://dx.doi.org/10.1007/s00128-015-1499-3

68. Pieper H, Chercheja S, Eigler S, Halbig CE, Filipovic MR, Mokhir A. Endoperoxides Revealed as Origin of the Toxicity of Graphene Oxide. Angew Chemie - Int Ed. 2016;55(1):405–7.

69. Ibelli T, Templeton S, Levi-Polyachenko N. Progress on utilizing hyperthermia for mitigating bacterial infections. Int J Hyperth [Internet]. 2018;34(2):144–56. Available from: https://doi.org/10.1080/02656736.2017.1369173

70. Wu X, Li H, Xiao N. Advancement of Near-infrared (NIR) laser interceded surface

enactment of proline functionalized graphene oxide with silver nanoparticles for proficient antibacterial, antifungal and wound recuperating therapy in nursing care in hospitals. J Photochem Photobiol B Biol [Internet]. 2018;187(27):89–95. Available from: https://doi.org/10.1016/j.jphotobiol.2018.07.015

71. Shahnawaz Khan M, Abdelhamid HN, Wu HF. Near infrared (NIR) laser mediated surface activation of graphene oxide nanoflakes for efficient antibacterial, antifungal and wound healing treatment. Colloids Surfaces B Biointerfaces [Internet]. 2015;127:281–91. Available from: http://dx.doi.org/10.1016/j.colsurfb.2014.12.049

72. Feng Y, Chen Q, Yin Q, Pan G, Tu Z, Liu L. Reduced Graphene Oxide Functionalized with Gold Nanostar Nanocomposites for Synergistically Killing Bacteria through Intrinsic Antimicrobial Activity and Photothermal Ablation. ACS Appl Bio Mater. 2019;2(2):747–56.

73. Cheng YW, Wang SH, Liu CM, Chien MY, Hsu CC, Liu TY. Amino-modified graphene oxide nanoplatelets for photo-thermal and anti-bacterial capability. Surf Coatings Technol [Internet]. 2020;385(January):125441. Available from: https://doi.org/10.1016/j.surfcoat.2020.125441

74. Ma G, Qi J, Cui Q, Bao X, Gao D, Xing C. Graphene oxide composite for selective recognition, capturing, photothermal killing of bacteria over mammalian cells. Polymers (Basel). 2020;12(5):1–14.

75. Zhang Q, Liu X, Tan L, Cui Z, Li Z, Liang Y, et al. An UV to NIR-driven platform based on red phosphorus/graphene oxide film for rapid microbial inactivation. Chem Eng J [Internet]. 2020;383(July 2019):123088. Available from: https://doi.org/10.1016/j.cej.2019.123088

76. Li Y, Liu X, Tan L, Cui Z, Yang X, Zheng Y, et al. Rapid Sterilization and Accelerated Wound Healing Using Zn2+ and Graphene Oxide Modified g-C3N4 under Dual Light Irradiation. Adv Funct Mater. 2018;28(30):1–12.

77. Wang YW, Fu YY, Wu LJ, Li J, Yang HH, Chen GN. Targeted photothermal ablation of pathogenic bacterium, Staphylococcus aureus, with nanoscale reduced graphene oxide. J Mater Chem B. 2013;1(19):2496–501.

78. Kaushal S, Pinnaka AK, Soni S, Singhal NK. Antibody assisted graphene oxide coated gold nanoparticles for rapid bacterial detection and near infrared light enhanced

antibacterial activity. Sensors Actuators, B Chem [Internet]. 2021;329(August):129141. Available from: https://doi.org/10.1016/j.snb.2020.129141

79. Kainz K, Bauer MA, Madeo F, Carmona-Gutierrez D. Fungal infections in humans: The silent crisis. Microb Cell. 2020;7(6):143–5.

80. Díez-Pascual AM. Antibacterial action of nanoparticle loaded nanocomposites based on graphene and its derivatives: A mini-review. Int J Mol Sci. 2020;21(10).

81. Liu S, Zeng TH, Hofmann M, Burcombe E, Wei J, Jiang R, et al. Antibacterial activity of graphite, graphite oxide, graphene oxide, and reduced graphene oxide: Membrane and oxidative stress. ACS Nano. 2011;5(9):6971–80.

82. Pavlovsky L, Sturtevant RA, Younger JG, Solomon MJ. Effects of temperature on the morphological, polymeric, and mechanical properties of Staphylococcus epidermidis bacterial biofilms. Langmuir. 2015;31(6):2036–42.